A MUltidimensional Compliant Decoupled Actuator (MUCDA) for Pelvic Support during Gait

Dario Wyss, *Member, IEEE,* Andrew Pennycott, Volker Bartenbach, Robert Riener, *Member, IEEE,* and Heike Vallery, *Member, IEEE,*

***Abstract*—Series Elastic Actuation decouples actuator inertia from the interaction ports and is thus advantageous for force-controlled devices. Parallel or even passive compliance can fulfill a complementary role by compensating for gravitational or periodic inertial forces or by providing passive guidance. Here, these concepts are combined in an underactuated six degree of freedom (DoF) compliant manipulator with one actuated DoF. The mechanism comprises a spring assembly in which each spring serves as an actuation element and simultaneously provides passive compliance in the unactuated DoF. The device is designed to assist weight shifting via controlled lateral forces on a human pelvis during treadmill walking and its eigenfrequencies are tuned to align with normal gait. Six-DoF force and torque sensing are realized via a model of the spring deformation characteristics in combination with low-cost inertial and optical sensors. Experimental evaluation demonstrates that the system can effectively follow physiological lateral pelvis movement with low interaction forces and also has little impact on remaining pelvis motions.**

***Index Terms*—Series Elastic Actuator, Rehabilitation, Haptics**

I. Introduction

The traditional approach to robotics has tended to emphasize serial kinematic structures and stiff actuation which, although suitable for many position control tasks found in manufacturing, is not ideal for applications that require transparent force control, due to undesired inertial effects. Particularly in haptics, in which robots operate in direct contact with humans, control over robot-human interaction forces in six degrees of freedom (DoF) is critical for safe operation.

An important area of application for highly transparent robotic interfaces is the field of rehabilitation robotics. A robotic interface able to render low impedance can enhance active patient participation and achieve low robotic interference whilst retaining the option of more support when needed [1]. Gait training represents a particularly important area of rehabilitation for stroke survivors [2] and individuals with spinal cord injury [3]. The human pelvis moves in a six DoF pattern during normal gait [4], the kinematics of which can be represented as periodic oscillations in the range of 1-2 Hz in able-bodied individuals [5]. The pelvis translates in longitudinal, lateral and vertical directions in an approximately sinusoidal manner. The lateral direction has the greatest amplitude of around 20 mm. The orientation of the pelvis is governed by three angles [6] that influence the vertical position of the center of mass during gait [7]. In addition to control of angular momentum in the sagittal plane [8], balancing during walking is a crucial element of human gait involving weight shifting from one leg to the other in the lateral direction (i.e. the frontal plane) [9]. During walking, the center of mass constantly moves outside the base of support, and must be actively stabilized through foot placement [10]. As such, the lateral degree of freedom has an important role to play during walking and it could be argued that it should be afforded particular attention during design of robotic devices for rehabilitation.

Restraining the pelvis adversely affects gait dynamics [11] and thereby may impede the rehabilitation process in stroke survivors [12]. Therefore, designers of modern gait rehabilitation robots generally incorporate multiple DoF for pelvis motion. For example, the LOPES II treadmill-based exoskeleton [13] features two actuated (lateral and forward/backward translation) and four passive (one vertical and three rotational) DoF for the pelvis. Another pelvis manipulator mounted on a moving cart, the KineAssist [14], supports users at the pelvis and enables unrestricted and highly transparent pelvis rotations about all three axes as well as vertical translation. Horizontal translations are enabled via the device's moving frame. Both aforementioned devices use stiff design and closed-loop force control, which can partially mitigate unwanted effects by reducing the robot's reflected inertia [15], [16]. In LOPES II, the stiff design in combination with force sensors allows rendering masses at the pelvis which are lower than the actual structural masses of the device components. For the KineAssist, given the high mass and inertia of the frame, transparency is more difficult to achieve for the translational DoF. The extent of inertia reduction for stiff robots remains limited [16], and the required force sensors tend to substantially increase cost.

For reducing mass and inertia, most dedicated pelvis actuation devices rely on parallel actuation to enable transparent interaction during the six-dimensional pelvic movement: a number of rigid or elastic members such as cables, rods, or springs are each connected to the pelvis on one end, and to a fixed frame on the other. Varying numbers of these members are actuated to change their length, for example six in the A-TPAD [17] or in PAM [18], three in the BAR [19], and one in a dedicated 1-DoF pelvis perturbator [20].

In underactuated parallel manipulators, the design-inherent

D. Wyss, V. Bartenbach and A. Pennycott are with the Sensory-Motor Systems Lab, Institute of Robotics and Intelligent Systems, ETH Zurich.

H. Vallery (corresponding author) is with the Faculty of Mechanical, Maritime and Materials Engineering, Delft University of Technology (h.vallery@tudelft.nl).

R. Riener is head of the Sensory-Motor Systems Lab, ETH Zurich. He is also with the Spinal Cord Injury Center, University Hospital Balgrist, Medical Faculty, University of Zurich.

coupling of DoF can be an issue. For example, to assist only in weight shifting i.e. to apply lateral forces, the standard paradigm of parallel actuation would involve one single member as in [20], or an antagonistically arranged pair of members connected to a fixed base. While this enables free movement in five of the six DoF, such a mechanism does not allow the applied forces to be perfectly lateral. Instead, force components can occur in other directions as well as moments about all axes. This can be alleviated by connecting the members not to a fixed base, but rather to moving points that passively follow major pelvis movement, particularly anterior-posterior movement [21]. However, this further complicates the design and still does not ensure full decoupling of DoF.

Both in series and parallel manipulators, the incorporation of physical compliance of diverse type is now an established design strategy to achieve high-fidelity force and impedance control [22]. The Series Elastic Actuator (SEA) is a prominent example of the use of physical compliance to improve force control. Its key feature is an elastic element in series with a stiff actuator [23]. The concept transforms force control into a position control task because the deflection of the elastic element acts as an indirect force measurement. Although the elastic element lowers the overall bandwidth and inhibits stiff actuation [24], its effect is favorable for many applications [25], [26] as it allows back-drivability and limits mechanical impedance, and thereby contributes to the safety and comfort for operation with humans [27]. While most SEAs have hitherto had a single DoF, the present authors have demonstrated two extension concepts to realize SEA manipulators with multiple DoF, both applied to gait training. The first extension was fully actuated and involved placing a stiffly actuated n-DoF robot in series with a single end-effector module that is elastic in the same n DoF and rigid in the $6-n$ others. It was applied to a gait training robot for rats that actuated four DoF of the animal's trunk (translations and yaw) and constrained the two others (pitch and roll) to enforce upright gait [28]. Interacting with humans, it is less beneficial to constrain rotational DoF as these may interfere with natural motion. Therefore, a second extension was an underactuated SEA-based cable robot that transmits a single force vector to a human trunk by means of a harness, while not imposing kinematic rotational constraints [29].

Passive compliant elements such as springs are routinely applied to compensate for constant (e.g. gravitational) forces. Furthermore, passive compliance can allow some freedom around an equilibrium configuration without enabling excessive deviation from this point, for example, to provide guidance. With appropriate tuning, passive compliance can also compensate for periodic inertial forces [30].

In this article, a six-DoF end-effector mechanism is proposed that achieves decoupling of actuated and unactuated DoF by unifying the concepts of passive compliance and serial elasticity: the MUltidimensional Compliant Decoupled Actuator (MUCDA). The MUCDA exhibits series elastic actuation in one constant direction only, and fully passive elasticity in the remaining five DoF. This decoupling is enabled by means of a linear actuator in combination with an assembly of multiple individual coil springs. Each spring in the assembly provides serial and passive elasticity, thus minimizing overall mass and complexity.

The MUCDA is realized and experimentally evaluated in a gait rehabilitation platform that interacts with the human pelvis in six DoF. A single actuated DoF allows the crucial task of lateral weight shifting to be supported to differing degrees according to the walking abilities of the user - for more able walkers, the device can be transparent, but more guidance can be provided by the machine when required. Compliance in the remaining five DoF keeps the user in a safe range around the origin position without restriction to a fixed point in space. This combination of passive compliance and the SEA concept leads to high transparency in all six DoF, which is expected to encourage a higher degree of active participation and thereby more positive gait training outcomes.

II. Hardware Concept

The system, shown in Fig.1, is designed such that it actively guides the human pelvis to support lateral weight shift during treadmill walking, while providing only minimal passive support to the remaining DoF of the pelvis. The aim is thus to support and guide the human pelvis without completely restraining it. The support should hold the user approximately in position without interfering with physiological movements, including arm swing.

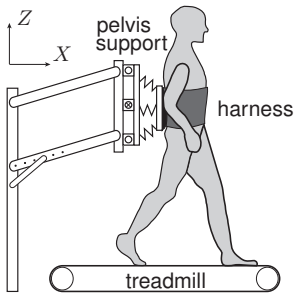

Fig. 1. System overview

The MUCDA concept is applied to fulfill these requirements. A single motor is used to support lateral weight shifting and produces a configuration with five passive and one actuated DoF. The MUCDA pelvis module comprises two functional groups - an actuated element and a passive component - as summarized in Fig. 2. An actuator and linear guides are placed between a fixed and a middle plate in order to translate the latter component. This lateral translation is used to support the lateral movements of the user. The user is mechanically connected to the pelvis plate, which in turn is attached to the middle plate via a multi-DoF compliant module, which is an assembly of linear springs.

This spring assembly enables relative movements of the two plates with respect to each other. The elastic behavior of this connection - governed by the stiffness matrix - defines how users are influenced when moving their pelvis in all five unactuated DoF. In the lateral direction, the linear motor and the elasticity in this DoF together form a series elastic actuator.

The system comprises a frame connected to the environment via linear guides movable in the y-direction. The pelvis plate

This article has been accepted for publication in a future issue of this journal, but has not been fully edited. Content may change prior to final publication. Citation information: DOI 10.1109/TMECH.2018.2878289, IEEE/ASME Transactions on Mechatronics

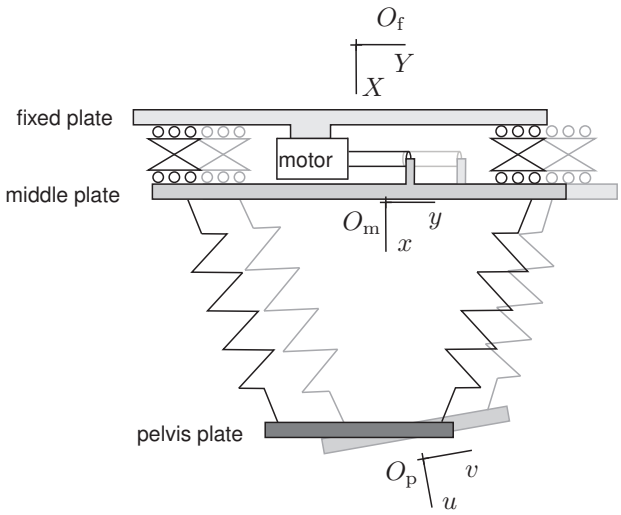

Fig. 2. Pelvis support module comprising: 1. the actuated module, where the middle plate translates in Y-direction relative to the fixed plate by linear guides and an actuator; 2. a passive module in which the pelvis plate follows the user's movements in six DoF and is connected by compliant components to the middle plate. Coordinate systems corresponding to the fixed, middle and pelvis plates are shown as O_f, O_m and O_p, respectively

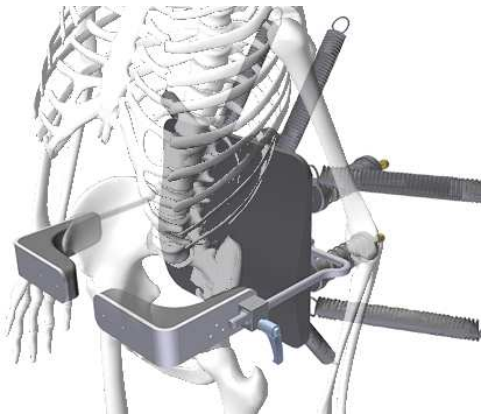

Fig. 3. User fixation on the pelvis module

is connected to the linear actuator using the spring assembly depicted in figure 4. The lateral DoF is actuated by a direct-drive electromagnetic linear motor (P01-48x240 from NTI AG LinMot, Spreitenbach, Switzerland). This actuator can produce forces and velocities of up to 585 N 1.7 m/s, respectively. This installed peak force is almost six times the amount expected for normal operation to enable stiff guidance near the end of the allowed workspace. An image of the pelvis module - showing the positions of the motor and linear guides as well as the fixed, middle and pelvis plates - is provided in Fig. 4.

Since the compliant behavior is realized through the pelvis module, the mechanical connection to the human user should be as stiff as possible. For comfort, the user wears a cushioned harness around the waist connected to leg loops that interface to the pelvis module as well as to an external body weight support system by adjustable straps. The moving plate of the pelvis module is padded with an anatomically formed foam. The user is secured to this pad over an adjustable bracket as

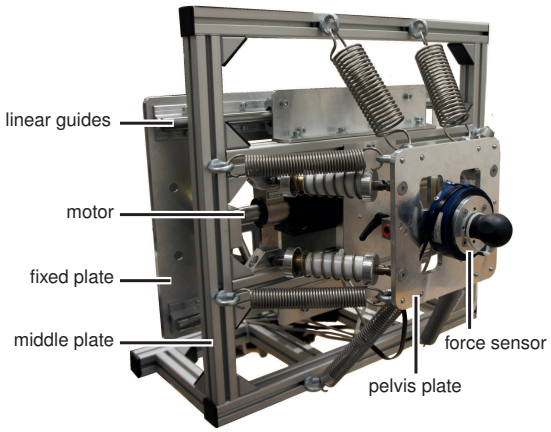

Fig. 4. Compliant pelvis module (with force-torque sensor for evaluation)

seen in Fig. 3. For the supporting frame and treadmill, slightly adjusted components of the Lokomat environment (Hocoma AG, Volketswil, CH) were used.

III. Design of the Passive Compliant Module

A. Desired Stiffness Matrix

The compliant module must fulfill stiffness requirements in different DoF derived from the physiological movement pattern of the human pelvis during walking. A second objective is to minimize the coupling between the various DoF by ensuring that the off-diagonal terms of the stiffness matrix are as close to zero as possible.

Pelvic motion is described by a set of six generalized coordinates $\boldsymbol{q}_\mathrm{p}$ with the three translational coordinates x_p, y_p, z_p of the pelvis center of mass and the zyx Euler angles θ_z, θ_y, θ_x. When the angles are zero, the x-axis points in the subject's anterior direction, y in the lateral direction (left with respect to the subject's perspective), and the vertical axis z in the subject's longitudinal axis direction. The angle θ_z denotes the transverse rotation (yaw) about the vertical z-axis, θ_y the tilt (pitch) angle about an intermediate y'-axis, and θ_x is the obliquity (roll) angle about the anterior-posterior u-axis. The forces and moments generated by the device on the user in the inertial coordinate directions are denoted F_x, F_y, F_z and M_x, M_y, M_z, respectively.

The main direction-specific objectives are:

- x-translation: the forward and backward motion of the user are to be constrained such that no low-frequency drift will occur, while still permitting some oscillation.
- y-translation: the resulting stiffness is chosen according to the desired performance of the SEA since the stiffness influences the bandwidth of the force controller and the achievable stiffness in impedance control.
- z-translation: any unwanted interaction forces caused by the device are to be avoided.
- θ_z-rotation: allow some freedom for users to deviate from a nominal configuration but keep them within a safe range of motion.

In the x-direction, the fundamental harmonic of human pelvis motion when walking on a treadmill must be enabled.

This oscillation has less than 2 cm amplitude [31]. More oscillation is not desired when used in combination with a body weight support system and exoskeletal legs mounted to the treadmill frame. The user should stay directly under the deflection pulley of the BWS. Therefore, we chose to associate an excursion of 1 cm with a force of 100 N, which is very difficult to resist as previously observed with the FLOAT robot [29]. A study by [32] even found lower values of forces that could not be resisted. This leads to a desired stiffness of 10000 N/m.

The y-direction is the only actuated DoF. To enable low interaction forces in zero-impedance control, the stiffness of the spring should be made as low as possible. However, the stiffness must be at least as high as the maximum expected virtual stiffness that will be rendered by an assistive controller [24]. From experience with balance assistance on a similar robot [33], we know that making use of feed-forward assistance, a relatively low stiffness of 3000 N/m is sufficient.

Reducing interaction forces in the vertical direction is particularly challenging when the module is used together with an active leg orthosis, which typically has a high inertia. As no active elements are present to compensate for robot dynamics, the passive structure itself must minimize the forces. To achieve this goal, the eigenfrequency of the oscillating mass-spring assembly must be in the same range as an average human gait frequency [30]. The medium walking cadence is expected to be $f_0 = 0.75\,\mathrm{Hz}$ and the estimated mass of the oscillating parts of the device $m = 33.6\,\mathrm{kg}$, which is mainly caused by the mass of an additional exoskeletal structure for the legs, giving a resulting stiffness k_z equal to $m\omega_0^2$.

Rotational stiffness about the z-axis was chosen such that yaw rotation would be constrained, in order to avoid crossing legs on the treadmill, using a relatively high stiffness of 100 Nm/rad. We chose the same value also for the two other rotational DoF.

The stiffness matrix $\mathbf{K}_\mathrm{c}$ has the matrix form:

$$\mathbf{K}_\mathrm{c} = -\begin{bmatrix} \frac{\partial F_x}{\partial x_\mathrm{p}} & \frac{\partial F_x}{\partial y_\mathrm{p}} & \cdots & \frac{\partial F_x}{\partial \theta_z} \\ \frac{\partial F_y}{\partial x_\mathrm{p}} & \frac{\partial F_y}{\partial y_\mathrm{p}} & \cdots & \frac{\partial F_y}{\partial \theta_z} \\ \vdots & \vdots & \ddots & \vdots \\ \frac{\partial M_z}{\partial x_\mathrm{p}} & \frac{\partial M_z}{\partial y_\mathrm{p}} & \cdots & \frac{\partial M_z}{\partial \theta_z} \end{bmatrix} \tag{1}$$

Summarizing the requirements for the individual DoF, the desired numerical values for the stiffness matrix $\mathbf{K}_{\mathrm{c,des}}$ are:

$$\mathbf{K}_{\mathrm{c,des}} = \mathrm{diag}\,(10000, 3000, 723, 100, 100, 100) \tag{2}$$

Units are N/m and Nm/rad for the respective entries.

B. Spatial Stiffness Synthesis

The spring assembly needs at least six individual springs for its six DoF, and the stiffnesses and configuration of the springs need to be determined from the desired stiffness matrix.

Huang and Schimmels introduced a screw theory-based numerical method to synthesize a desired stiffness matrix [34]. A prerequisite is that the off-diagonal terms of the stiffness matrix be zero; a further drawback of the method is that the stiffness matrix is valid only for one chosen point and can greatly change due to small deviations from this point. The stiffness matrix would ideally remain constant over the workspace of the end-effector but the deviations from the origin are not negligible. In addition, further constraints arise from practical considerations: for instance, the device must not interfere with the user's movements, especially concerning arm swing [35].

Therefore, an alternative approach was selected to determine the attachment points of the springs and their corresponding spring constants. This intuitive approach decomposes the three-dimensional problem into three two-dimensional problems as seen in Fig. 5. For each of these two-dimensional problems, the attachment points for four simple springs were found through geometric considerations and the spring stiffnesses and resting lengths were calculated via parameter optimization. The number of springs used and their attachment points on both plates were chosen to fulfill the space limitations and to achieve symmetry. Consequently, twelve springs were used in total, comprising four compression springs and eight tension springs. As few as possible compression springs are used since peripheral mechanics (i.e. two universal joints and a linear guide) are needed for these springs, which introduces additional weight into the system.

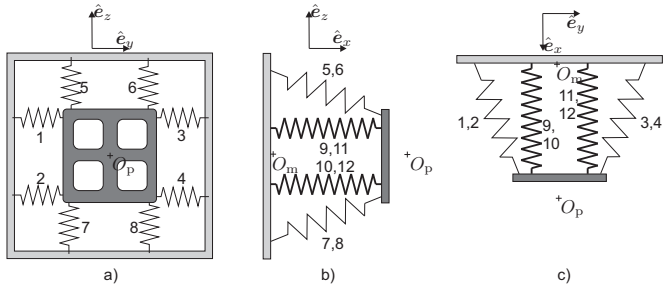

Fig. 5. Geometric decomposition of the 3D problem into three 2D problems. Thin lines represent tension springs, bold lines

Springs 1 - 4, shown as projections in the z-y plane as in Fig. 5a) serve to create the elasticity in lateral direction, while springs 5 - 8 perform the same function in the vertical direction. These springs also influence the rotational elasticity around the x-axis. The compression springs 9 - 12 in Fig. 5 act mainly in the x-direction but cover also the rotations about the y and z-axes. This arrangement of the springs minimally interferes with other motions of the user.

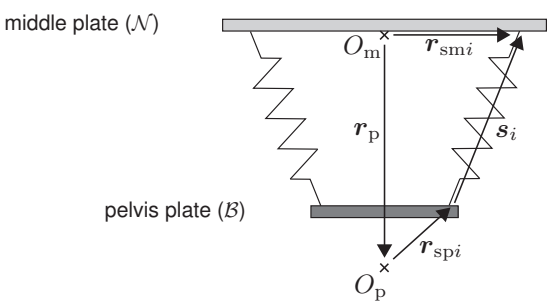

Fig. 6. Definition of vectors describing spring geometry.

To perform the optimization procedure to determine the

individual spring characteristics, the stiffness matrix must be written as a function of the spring stiffnesses and resting lengths. As shown in Fig. 6, each spring i, $i = 1...n$ has an attachment point on the pelvis plate of position vector $\boldsymbol{r}_{\mathrm{p}}+\boldsymbol{r}_{\mathrm{sp}i}$ with respect to O_{m}. The attachment point of the same spring on the middle plate has position vector $\boldsymbol{r}_{\mathrm{sm}i}$ with respect to O_{m}.

An inertial frame $\mathcal{N}$ uses a set of direction vectors $\hat{\boldsymbol{e}}_x$, $\hat{\boldsymbol{e}}_y$, and $\hat{\boldsymbol{e}}_z$ connected to the middle plate. Because the middle plate does not rotate, these and the relative position vectors $\boldsymbol{r}_{\mathrm{sm}i}$ are constant. A frame $\mathcal{B}$ is connected to the pelvis plate and rotates with the human pelvis. The rotation matrix ${}^{\mathcal{N}}\mathbf{C}_{\mathcal{B}}$ describes the orientation of the human pelvis and thereby the pelvis plate with respect to the middle plate by mapping vectors with components expressed in the pelvis-fixed $\mathcal{B}$-frame to the inertial $\mathcal{N}$-frame.

Vector addition can be used to express the vector pointing along the i-th spring as:

$$ {}^{\mathcal{N}}\boldsymbol{s}_i = {}^{\mathcal{N}}\boldsymbol{r}_{\mathrm{sm}i} - {}^{\mathcal{N}}\boldsymbol{r}_{\mathrm{p}} - {}^{\mathcal{N}}\mathbf{C}_{\mathcal{B}} \cdot {}^{\mathcal{B}}\boldsymbol{r}_{\mathrm{sp}i}. \tag{3}$$

The associated spring force $\boldsymbol{F}_i$ that the i-th spring exerts on the moving plate is given by

$$ \boldsymbol{F_i} = k_i(|\boldsymbol{s}_i| - l_{0i})\frac{\boldsymbol{s}_i}{|\boldsymbol{s}_i|} \tag{4}$$

and the spring's moment vector $\boldsymbol{M}_i$ with respect to the pelvis center O_{p} as

$$ {}^{\mathcal{N}}\boldsymbol{M_i} = ({}^{\mathcal{N}}\mathbf{C}_{\mathcal{B}} \cdot {}^{\mathcal{B}}\boldsymbol{r}_{\mathrm{sp}i}) \times {}^{\mathcal{N}}\boldsymbol{F_i}, \tag{5}$$

with l_{0i} as resting length of the i-th spring.

Based on these equations, forces and moments acting on the pelvis can be compactly written as

$$ \boldsymbol{\tau} = \mathbf{A}\boldsymbol{p}, \tag{6}$$

whereby the parameter vector $\boldsymbol{p}$ is a function of stiffnesses k_i and resting lengths l_{0i}:

$$ \boldsymbol{p} := \begin{bmatrix} k_1 & k_2 & ... & k_n & k_1 l_{01} & k_2 l_{02} & ... & k_n l_{0n} \end{bmatrix}^{\mathrm{T}}, \tag{7}$$

the vector $\boldsymbol{\tau}$ subsumes the generalized forces of all $n = 12$ springs

$$ \boldsymbol{\tau} := \begin{bmatrix} \sum_{i=1}^{n} \boldsymbol{F}_i \\ \sum_{i=1}^{n} \boldsymbol{M}_i \end{bmatrix}^{\mathrm{T}}, \tag{8}$$

and the matrix $\mathbf{A}$ encodes the geometric configuration:

$$ \mathbf{A} := \begin{bmatrix} \boldsymbol{s}_1 & ... & \boldsymbol{s}_n & \frac{\boldsymbol{s}_1}{|\boldsymbol{s}_1|} & ... & \frac{\boldsymbol{s}_n}{|\boldsymbol{s}_n|} \\ \boldsymbol{a}_1 & ... & \boldsymbol{a}_n & \frac{\boldsymbol{a}_1}{|\boldsymbol{s}_1|} & ... & \frac{\boldsymbol{a}_n}{|\boldsymbol{s}_n|} \end{bmatrix}, \tag{9}$$

with entries

$$ \boldsymbol{a}_i := \boldsymbol{r}_{\mathrm{sp}i} \times \boldsymbol{s}_i. \tag{10}$$

This optimization problem is linear in the parameters, and therefore, linear least-squares optimization is applied to find the optimal parameter vector $\boldsymbol{p}$ such that the forces and moments subsumed in $\boldsymbol{\tau}$ match a desired spatial profile $\boldsymbol{\tau}_{\mathrm{des}}(\boldsymbol{q}_{\mathrm{p}})$, which is a function of the pelvis generalized coordinates $\boldsymbol{q}_{\mathrm{p}}$. The training data $\boldsymbol{\tau}_{\mathrm{des}}(\boldsymbol{q}_{\mathrm{p}})$ for this optimization is generated in form of a grid with boundaries and resolution summarized in Table I using the desired diagonal stiffness matrix.

Coordinate	Boundaries	Resolution	Unit
p_x	$\pm$ 20	1	mm
p_y	$\pm$ 30	1	mm
p_z	$\pm$ 50	1	mm
θ_x	$\pm$ 10	0.1	deg
θ_y	$\pm$ 2	0.1	deg
θ_z	$\pm$ 10	0.1	deg

TABLE I
BOUNDARIES AND RESOLUTION FOR THE OPTIMIZATION GRID

To map the individual spring stiffnesses to the stiffness matrix $\mathbf{K}_{\mathrm{c}}$ in end-effector space, the Jacobian matrix is used. Given a vector of individual spring lengths $\boldsymbol{L} = \begin{bmatrix} l_1 & l_2 & \dots & l_i \end{bmatrix}^{\mathrm{T}}$, which in turn depends on the position vector $\boldsymbol{r}_{\mathrm{p}}$, the Jacobian matrix $\mathbf{J}$ is defined as:

$$ \mathbf{J} = \frac{\partial \boldsymbol{L}}{\partial \boldsymbol{r}_{\mathrm{p}}} = \begin{bmatrix} \frac{\partial l_1}{\partial x_{\mathrm{p}}} & \frac{\partial l_1}{\partial y_{\mathrm{p}}} & \frac{\partial l_1}{\partial z_{\mathrm{p}}} & \frac{\partial l_1}{\partial \theta_x} & \frac{\partial l_1}{\partial \theta_y} & \frac{\partial l_1}{\partial \theta_z} \\ \frac{\partial l_2}{\partial x_{\mathrm{p}}} & \frac{\partial l_2}{\partial y_{\mathrm{p}}} & \frac{\partial l_2}{\partial z_{\mathrm{p}}} & \frac{\partial l_2}{\partial \theta_x} & \frac{\partial l_2}{\partial \theta_y} & \frac{\partial l_2}{\partial \theta_z} \\ \vdots & & & & & \\ \frac{\partial l_i}{\partial x_{\mathrm{p}}} & \frac{\partial l_i}{\partial y_{\mathrm{p}}} & \frac{\partial l_i}{\partial z_{\mathrm{p}}} & \frac{\partial l_i}{\partial \theta_x} & \frac{\partial l_i}{\partial \theta_y} & \frac{\partial l_i}{\partial \theta_z} \end{bmatrix} \tag{11}$$

With the individual spring stiffnesses k_i being contained in matrix $\mathbf{K}_{\mathrm{s}}$:

$$ \mathbf{K}_{\mathrm{s}} := \mathrm{diag}\left(k_1, k_2, \dots, k_n\right), \tag{12}$$

the stiffness matrix $\mathbf{K}_{\mathrm{c}}$ is

$$ \mathbf{K}_{\mathrm{c}} = \mathbf{J}^{\mathbf{T}}\mathbf{K}_{\mathrm{s}}\mathbf{J}. \tag{13}$$

Table II shows the characteristics for the actually chosen physical springs that are used in the hardware realization.

Spring	Initial lengths	stiffness
$1-4$	0.196 m	1577 N/m
$5-8$	0.161 m	628 N/m
$9-12$	0.19 m	1680 N/m

TABLE II
SPRING CHARACTERISTICS

The resulting stiffness matrix $\mathbf{K}_{\mathrm{c,opt}}$ with the actual springs (which has the same units as above) is:

$$ \mathbf{K}_{\mathrm{c,opt}} = \begin{bmatrix} 11134 & 0 & 0 & 0 & 0 & 0 \\ 0 & 3379 & 0 & 0 & 0 & 91 \\ 0 & 0 & 1017 & 0 & 28 & 0 \\ 0 & 0 & 0 & 79 & 0 & 0 \\ 0 & 0 & 28 & 0 & 85 & 0 \\ 0 & 91 & 0 & 0 & 0 & 126 \end{bmatrix} \tag{14}$$

The maximum workspace is determined by the maximum excursion of the springs and by physical endstops. It is verified that the device can also accommodate users who exhibit pathological (excessive) pelvis motions when walking freely. The workspace boundaries are shown in Table III, together with the forces occurring at these boundaries, for the case of single-DoF excursions from the neutral position. The limits of the workspace cannot be reached during walking due to the high forces occurring there. In the lateral direction, forces as low as 40-60 N cannot be resisted anymore [32].

Note that the device is not meant to support weight of a person or to catch a person when falling. During gait rehabilitation training, such tasks would be realized via an external body weight support system.

Direction	Workspace	Max Force / Torque
x	-40 mm, +156 mm	-445 N, +1742 N
y	$\pm$ 214 mm	723 N
z	$\pm$ 288 mm	523 N
rot x	$\pm$ 27 °	$\pm$ 71 Nm
rot y	$\pm$ 39 °	$\pm$86 Nm
rot z	$\pm$ 39 °	$\pm$86 Nm

TABLE III
WORKSPACE OF THE PELVIS MODULE

IV. SENSING AND CONTROL

The absolute position and orientation of the MUCDA's end-effector are determined via a miniature camera module and a six-DoF inertial measurement unit (IMU) as depicted in Fig. 7. The low-cost camera is equipped with a filter permeable only to infrared light and tracks an array of four active infrared markers (LEDs) mounted on the pelvis plate. The maximal spatial and temporal resolutions are 100 Hz and 0.14 mm, respectively. The image sensor (PixArt Imaging Inc.) is equipped with custom-made peripherals in order to read the information via serial bus. The obtained image of 128 x 96 pixel resolution is oversampled onboard to generate a 1024 x 768 resolution view. The IMU (MPU9250, Invensense, San Jose, USA) uses a three-axis accelerometer along with a three-axis gyroscope and is sampled at a frequency of 1 kHz.

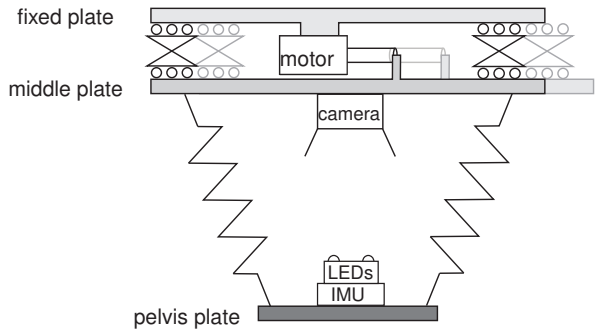

Fig. 7. Sensing system with IMU, infrared camera and infrared LED-array

A multiplicative quaternion extended Kalman filter, which provides fast and reliable sensing of the end-effector position and orientation, is used to combine the IMU and camera data to estimate the position and orientation of the pelvis plate. The linear actuator has an incremental encoder for its displacement with a resolution of 0.05 mm and has an additional linear potentiometer for calibration.

A cascaded approach with inner proportional velocity loop and outer PI force control loop is applied, as often employed in unidimensional SEAs [36], [24]. The inner velocity loop is integrated into the motor drive, enabling a high sampling rate of 20 kHz; the external force loop is executed on a Matlab xPC target PC with a sampling rate of 1 kHz.

V. EVALUATION PROTOCOL

To validate the sensing concept and to evaluate the performance of the system, additional external sensor systems were used in the set-up as described below. Additionally, to evaluate the system concerning its interaction with the pelvis during gait, an experiment with a human subject was conducted.

A. Mechanical Stiffness Verification

To investigate the stiffness matrix and the achievable lateral transparency, tests were conducted using an evaluation setup consisting in a pelvis support system, an optical tracking system and a six-DoF force-torque sensor mounted on the pelvis plate. The external multi-axis force-torque sensor was the model 45E15A4 from manufacturer JR3 (JR3 Inc., Woodland, USA). The measurement range is $\pm$ 200 N for F_y and F_z with a resolution of 0.025 N, and $\pm$ 200 N for F_x with a resolution of 0.05 N.

The optical tracking system (Qualisys AB, Gothenburg, Sweden, Oqus camera series) comprising four cameras provided a spatial resolution of 0.5 mm and covered the entire range of motion of the system. The force data was captured at a frequency of 1 kHz and filtered with a lowpass second-order Butterworth filter with a cutoff frequency of 50 Hz, applied firstly in the forward and then in the backward direction for zero phase shifting. The position data was captured at a frequency of 1 kHz, while the calibration of the Qualysis system indicated a spatial accuracy of 0.5 mm.

The calculated stiffness matrix was validated by blocking the lateral DoF of the pelvis module (so that the springs have to deflect to let the pelvis plate move in Y-direction) and by recording the forces and torques using the external six-DoF sensor and the position and orientation in 3D space.

External forces were induced into the system by manually moving the handle in 3D space, up to approximately 100 N and 10 Nm in all directions, respectively, corresponding to the maximum expected range of motion during normal operation. The precise range of the evaluation data is shown in Table IV.

Direction	Range of Motion
x	$\pm$ 9 mm
y	$\pm$ 24 mm
z	$\pm$ 43 mm
rot x	$\pm$ 4 °
rot y	$\pm$ 6 °
rot z	$\pm$ 6 °

TABLE IV
RANGE OF MOTION FOR VALIDATION

All movements were conducted slowly so as to minimize the effects of dynamic forces on the results. It was verified that the pelvis plate acceleration plate did not exceed 0.1 g.

The stiffness matrix was estimated from the external force and position sensor data by computing mean values over the range of motion.

B. Sensor Performance Evaluation

The performance of the position sensor was evaluated by comparing the internally calculated position data with the reference data from the optical tracking system. Similarly, the forces estimated from these positions in combination with the modeled spring characteristics were compared to the measurements of the external reference force sensor (shown in Fig. 4). Root mean square errors were calculated both for forces and positions. The same data set used to calculate the stiffness matrix was also employed for a quasi-static performance evaluation. In addition, dynamic measurements

were conducted by manually moving the force sensor attached to the pelvis plate in all DoF with up to 3 Hz for 25 seconds. The range of motion is denoted in Table IV.

C. Closed-Loop Performance Evaluation

First, to quantify the transparency of the module in the (lateral) Y-direction, the pelvis module was unblocked and the control system was activated in zero-impedance mode. The handle was then manually moved around in a periodic manner from left to right at different speeds and the lateral (Y-direction) force and position data were recorded.

The resulting data was used to estimate the parameters of a dynamic equation that describes the reflected end effector mass m_v and damping d_v perceived at the pelvic plate according to

$$F_{u,Y} = m_v \cdot \ddot{Y}_p + d_v \cdot \dot{Y}_p. \tag{15}$$

in which $F_{u,Y}$ is the force applied by the user in Y-direction. The coefficients of the equation were estimated using linear regression. The position data were not filtered, while the velocity and acceleration were derived from low-pass-filtered position data using a second-order Butterworth filter with cutoff frequency 5 Hz, again applied in backward and forward directions to avoid phase shifting.

Second, a force-tracking experiment was conducted to evaluate force tracking performance, with the end effector being manually restrained and the force controller commanded to a reference sinusoidal force varying both in amplitude and frequency. Frequency slowly increased from 0.1 Hz to 10 Hz, while amplitude decreased with frequency from 40 N to 8 N. The recorded force estimate was then compared to the reference force in terms of phase lag and amplification in steady-state conditions for each frequency.

D. Usability Evaluation

A usability test with one male healthy subject (age: 31, height: 1.88 m, weight: 84 kg) was performed. The subject walked on a treadmill at 3 km/h without the device while the pelvic movements were assessed by the external optical tracking system. The subject then performed the task with the pelvis module attached to his pelvis, without body weight support. The marker clusters were placed on the spina iliaca anterior/superior, just above the user fixation of the pelvis module. The position data was first partitioned into 30 gait cycles by finding the maximum values of the first derivative of the Y-translation. Subsequently, the data was averaged across these gait cycles and the standard deviation was calculated.

VI. Results

A. Mechanical Stiffness Evaluation

The stiffness matrix $\mathbf{K}_{\mathrm{c,m}}$ obtained from the measured data comprising (mean values over the entire workspace) is

$$\mathbf{K}_{\mathrm{c,m}} = \begin{bmatrix} 10979 & 332 & 74 & 20 & 99 & 4 \\ 194 & 3160 & 25 & 8 & 18 & 71 \\ 376 & 155 & 1802 & 39 & 93 & 41 \\ 25 & 136 & 28 & 164 & 8 & 14 \\ 68 & 30 & 7 & 14 & 133 & 26 \\ 17 & 52 & 29 & 2 & 10 & 146 \end{bmatrix}. \tag{16}$$

The x- and y-directions are close to the design values, while in z-direction and for the rotations, the stiffness values are somewhat higher than desired.

B. Sensor Performance Evaluation

An excerpt of forces and moments as measured by the system's sensors and by the external reference sensors in dynamic conditions are shown in Fig. 8 [1]. The root mean

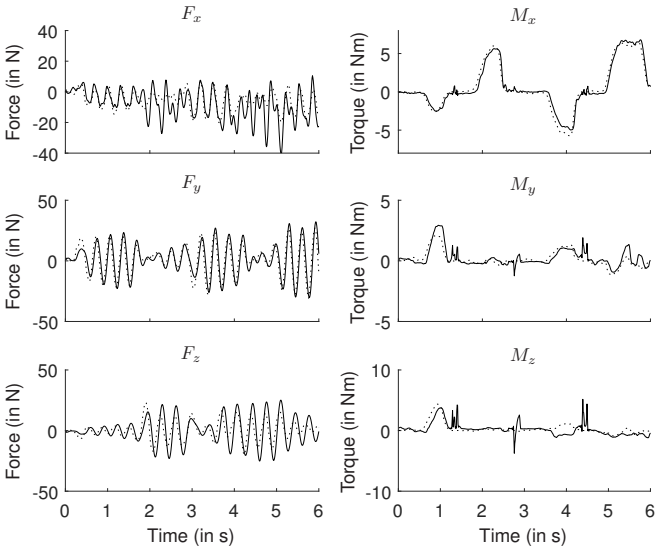

Fig. 8. Forces and torques calculated from the system's sensors (solid line) compared to an external reference force sensor (dotted line) during dynamic movements.

square values corresponding to the difference between the target and actual positions and forces across the entire static and dynamic data sets are shown in table V.

Direction	RMSE position		RMSE force	
	static	dynamic	static	dynamic
x	4.24 mm	1.10 mm	19.30 N	8.70 N
y	1.31 mm	2.60 mm	3.03 N	6.85 N
z	1.41 mm	2.87 mm	3.07 N	5.94 N
rot x	2.13 deg	3.43 deg	352 Nmm	473 Nmm
rot y	3.00 deg	4.20 deg	731 Nmm	868 Nmm
rot z	3.87 deg	4.98 deg	818 Nmm	912 Nmm

TABLE V
Root Mean Square Error (RMSE) of the position and force sensing system

C. Closed-Loop Performance Evaluation

The identified reflected virtual mass in Y-direction was $m_v = 3.6\,\mathrm{kg}$ and damping is $d_v = 14\,\mathrm{Ns/m}$, respectively. The corresponding R^2 value of 0.84 indicates a close fit of the model to the measured data.

Force tracking of the system is demonstrated in Fig. 9, in which measured and reference forces are shown for different frequencies. The experimental frequency response for force tracking is shown in Fig. 10, from which it is apparent that the bandwidth of the device is approximately 5 Hz. However,

[1] Data is available at https://doi.org/20.500.11850/297732

This article has been accepted for publication in a future issue of this journal, but has not been fully edited. Content may change prior to final publication. Citation information: DOI 10.1109/TMECH.2018.2878289, IEEE/ASME Transactions on Mechatronics

the phase at that frequency is already well beyond $-90°$, such that tracking of high-frequent references may not be possible with simple feedback controllers.

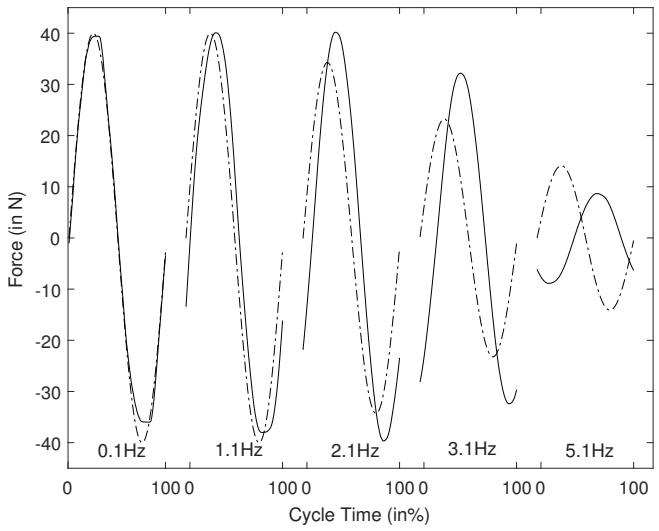

Fig. 9. Experimental tracking of the reference force. Reference values are dotted, measured forces in solid lines.

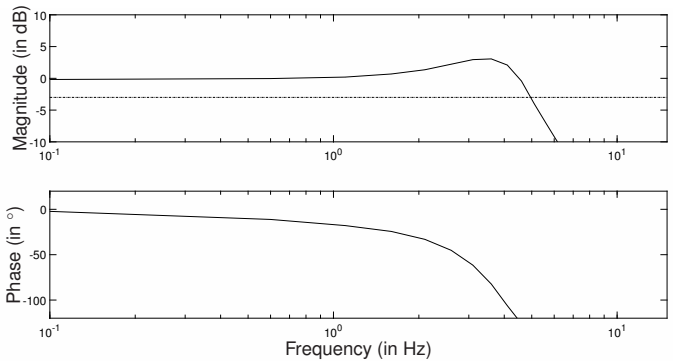

Fig. 10. Experimental tracking frequency response of the pelvis module.

D. Usability Test

The results of the two conditions of the usability test with and without the device are shown in Fig. 11. Fig. 12 shows the forces in the compliant module with their respective RMS errors. These errors were the deviation from the originally desired forces, as calculated with the desired stiffness matrix (2) for all DoF except for lateral translation, where the reference was zero force.

Movements in the three translational DoF as well as the rotation about the vertical axis appear to be little influenced by the human-robot interaction during walking. However, the pelvic tilt and obliquity rotations are less consistent, with both showing a decrease in amplitude with respect to free walking.

VII. Discussion

Through the application of a new type of compliant actuator with multidirectional series and passive elasticity (the MUCDA), a gait training platform has been realized. The

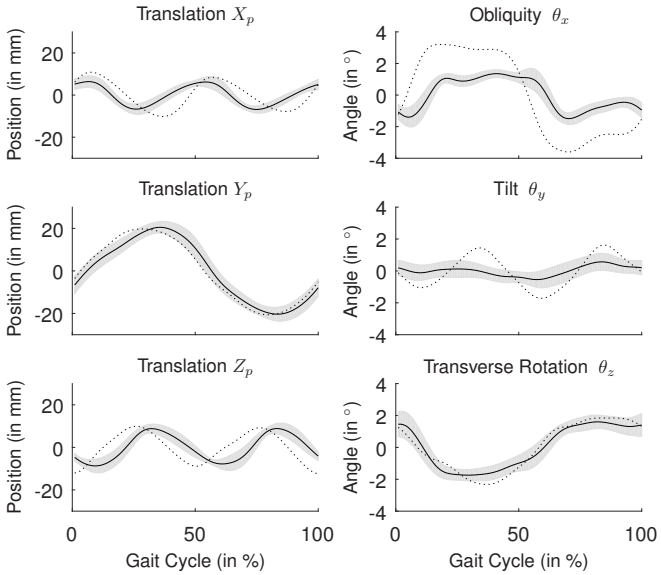

Fig. 11. Pelvic motions during usability test, with dotted lines representing the physiological motions when walking freely on the treadmill, solid lines lines representing the mean of the motions for 30 gait cycles of the same healthy subject with attached pelvis module. The gray area represents the standard deviation. Data was acquired with an external optical tracking system.

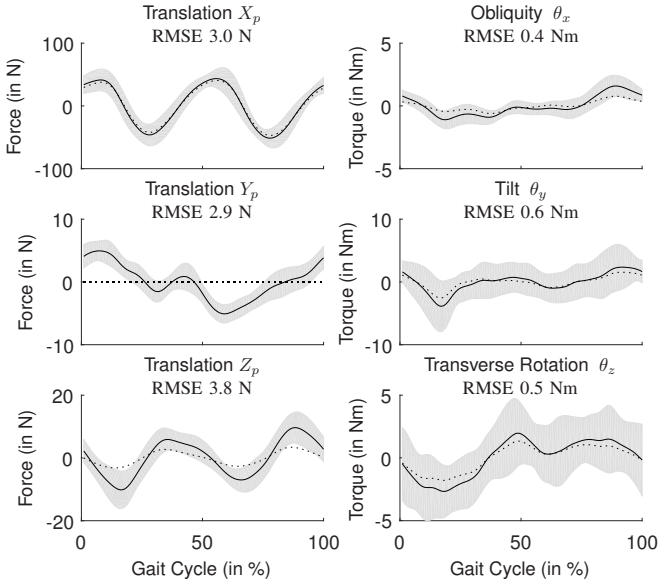

Fig. 12. Forces and torques in the pelvic interface. Dotted lines represent the desired forces according to desired stiffness matrix (2). Solid lines represent the forces and torques estimated by the observer, the gray area the standard deviation. RMSE forces indicate the deviation from the desired forces. Note the different scales.

proposed training device supports the posture and movement of a human user at the pelvis in all six DoF and actuates only weight shifting in the lateral direction.

The force and position sensing systems appear sufficiently reliable for the application. The force sensing errors in the $y-$ and z-directions were in the range of static friction, which was identified as 3.5 N in the y-direction and arises from the spring suspension system. The sensing error in the x-direction is due to the reduced accuracy of the tracking camera in this direction and the high stiffness in this direction, which tends to map small position errors to larger force errors.

Additionally, the results indicate that the device has very low reflected inertia. Although the reflected inertia in Y-direction is still higher than the one reported in [20], which is 1 kg, it is well below the 5.3 kg that can be added to the pelvis without significantly affecting gait [37]. The small forces occurring during the test can mostly be attributed to reflected damping. Consequently, the lateral interaction forces did not substantially influence pelvis kinematics. Despite the elastic interaction forces, amplitudes of the other translations as well as transverse rotation are not perceivably affected either. Only obliquity and tilt seem to be reduced in amplitude, due to the chosen stiffnesses and resulting moments. Particularly obliquity is a DoF in which strong pathological movements can occur, the so-called "hip-hiking" in stroke survivors. Depending on the training paradigm, reducing this movement to some extent via the spring forces may be desirable.

It can be seen that the relative phase of the three pelvis translations changes slightly when using the compliant module. This might be due to the compliance favoring a certain limit cycle that is not identical to the human pelvis motion. This effect would need to be further analyzed, and it could even be exploited in future designs, in order to favor certain desired (physiological) motions over others.

The training platform may require further modification in order to accommodate the differences from normal gait frequently shown by individuals post-stroke. This group frequently shows increased kinematic variability e.g. in swing and stride times [38], as well as different gait patterns arising from compensatory mechanisms such as a prolonged swing time [39], [40]. Nevertheless, it has been demonstrated that on average, individuals post-stroke have a walking cadence of as much as 80% that of able-bodied individuals [41]. Furthermore, the use of a spring to compensate for inertial effects of an exoskeleton is effective across a range of frequencies [30]: a spring structure demonstrably reduces vertical interaction forces even if the stiffness is not optimal. Therefore, despite being based on walking and step cadence data for able-bodied subjects, the proposed device should also be suitable for gait training for many individuals post-stroke.

The choice of the stiffness matrix entries for the passive DoF also depends on the adopted training paradigm. For example, some clinicians advocate constraining DoF in which pathological movements occur, such as hip hiking in obliquity. Others advocate leaving all DoF free that are not critical to the locomotor task and pose no safety risk during training. Because it is known that abnormal muscle activity does not necessarily cease even if the associated DoF is constrained during walking [42], the parameters in this paper were chosen closer to the latter paradigm. However, the proposed mechanical design principle can be equally used to adopt the former: For example, to fully suppress hip hiking passively, a higher stiffness would be desired for the fourth element on the diagonal of the stiffness matrix.

There is dispute about which DoF are most relevant to assist in pelvic movement of stroke survivors. For example, while [13] lists only lateral translation as a pelvis DoF that needs actuation, namely to assist balance, [43] advocates actuating obliquity instead to intervene with hip hiking. The actuation concept presented here can be adjusted to any other DoF by exchanging the motor and re-designing the stiffness matrix to desired values.

Though a single actuated DoF is considered in this article, the actuation concept could be extended to additional actuated DoF by keeping the same passive components while introducing more actuation on the input side. It would also be possible to place linear actuators in parallel to the springs. In the latter case, the individual spring elements serve as a series *and* parallel element to support the actuators, and possibly still act additionally as passive elastic components. Moreover, a particularly interesting property of elastic elements is their capacity to store potential energy. This is possible both in series and parallel configuration, whereby it depends on the specific task which configuration is more energy-efficient [44]. It remains to be investigated how the dual use of the springs in the MUCDA influences energetic aspects.

The sensing principle used in this device, consisting of a camera and an IMU, could also be replaced by alternative measurement methods. For example, recently it was shown that it is possible to precisely measure length of coil springs using their inductance [45]. In that case, the springs themselves could be used as sensors.

In this work, we only tested force tracking abilities of the pelvis manipulator with a simple force feedback controller and focus on zero-force tracking. Future research should address how to actuate weight shifting on a higher level when needed during therapy. One option would be to provide assistance (or challenge) in a low-frequent fashion, for example to tackle asymmetry by constant offset forces, or to guide periodic weight shifting from step to step. Given the low fundamental frequency of human lateral pelvis motion, the limited bandwidth of the compliant actuator should not pose a limitation. However, when attempting to apply impulsive forces on the pelvis, the simple force feedback controller may not suffice, and the reference force could be added to the motor as feed-forward term to improve force tracking. Impulsive forces could for example assist balance by inducing quick recovery movements. Previously, we had proposed a model-based control scheme that assisted lateral balance [33] using a modified Lokomat robot with lateral actuation. That controller was based on the concept of the extrapolated center of mass [46] or capture point [47]. Given that such a high-level controller is predictive, the low-level force controller can also be non-causal, further improving force tracking. Alternatively, one could choose stiffer springs, or switch from impedance control to open-loop position control of the motor, exploiting

the peak stiffness capabilities of the springs for more impulsive interaction.

In addition to guidance of the pelvis and possibly the legs, most individuals of the target group require partial support of their body weight during the single-support phase, which can be provided by an external body-weight-support system (BWS). Therefore, the system's harness was designed such that it can be used directly for this purpose. Vertical unloading with a conventional BWS can interfere with the dynamic balancing task [48], and so to avoid any such undesired stabilizing effects, a system able to translate laterally with the user is preferred [49].

VIII. Conclusion

The feasibility of assigning dual roles to elastic elements in order to unify series elastic actuation in selected DoF and passive compliance in other DoF has been demonstrated. The MUltidimensional Compliant Decoupled Actuator concept opens up new perspectives for actuators with tuned compliance for high-performance haptic devices. A prototype that exhibits highly compliant interactions with the dynamic movement of human gait has been conceived and realized, allowing controlled lateral forces on the pelvis, in combination with passive compliance in the other five DoF. Yet, functional benefits of lateral weight shifting assistance, as well as effectiveness for rehabilitation remain to be investigated.

Acknowledgment

The authors thank Michael Fritschi for developing the custom sensor technology. The contents of this publication were developed under the Marie-Curie career integration grant PCIG13-GA-2013-618899, under the grant KTI 11175.1 PFLS-LS Freewalk from the Swiss commission for technology and innovation, with the support of the Swiss National Science Foundation through the National Centre of Competence in Research on Robotics, and under two grants from the US Department of Education, NIDRR/NIDILRR grant numbers H133E070013 and 90RE5010 (formerly H133E120010).

References

[1] A. Pennycott, D. Wyss, H. Vallery, V. Klamroth-Marganska, and R. Riener, "Towards more effective robotic gait training for stroke rehabilitation: a review," *J Neuroeng Rehabil*, vol. 9, p. 65, 2012.

[2] P. Langhorne, J. Bernhardt, and G. Kwakkel, "Stroke rehabilitation," *The Lancet*, vol. 377, no. 9778, pp. 1693–1702, 2011.

[3] J. W. McDonald and C. Sadowsky, "Spinal-cord injury," *The Lancet*, vol. 359, no. 9304, pp. 417–425, 2002.

[4] V. Stokes, C. Andersson, and H. Forssberg, "Rotational and translational movement features of the pelvis and thorax during adult human locomotion," *Journal of Biomechanics*, vol. 22, no. 1, pp. 43–50, 1989.

[5] A. Barliya, L. Omlor, M. A. Giese, and T. Flash, "An analytical formulation of the law of intersegmental coordination during human locomotion," *Experimental brain research*, vol. 193, no. 3, pp. 371–385, 2009.

[6] R. Baker, "Pelvic angles: a mathematically rigorous definition which is consistent with a conventional clinical understanding of the terms," *Gait & posture*, vol. 13, no. 1, pp. 1–6, 2001.

[7] D. C. Kerrigan, P. O. Riley, J. L. Lelas, and U. Della Croce, "Quantification of pelvic rotation as a determinant of gait," *Archives of physical medicine and rehabilitation*, vol. 82, no. 2, pp. 217–220, 2001.

[8] R. R. Neptune and C. P. McGowan, "Muscle contributions to whole-body sagittal plane angular momentum during walking," *Journal of biomechanics*, vol. 44, no. 1, pp. 6–12, 2011.

[9] C. D. MacKinnon and D. A. Winter, "Control of whole body balance in the frontal plane during human walking," *Journal of biomechanics*, vol. 26, no. 6, pp. 633–644, 1993.

[10] C. E. Bauby and A. D. Kuo, "Active control of lateral balance in human walking," *Journal of biomechanics*, vol. 33, no. 11, pp. 1433–1440, 2000.

[11] J. F. Veneman, J. Menger, E. H. van Asseldonk, F. C. van der Helm, and H. van der Kooij, "Fixating the pelvis in the horizontal plane affects gait characteristics," *Gait & posture*, vol. 28, no. 1, pp. 157–163, 2008.

[12] J. Hidler, D. Nichols, M. Pelliccio, K. Brady, D. D. Campbell, J. H. Kahn, and T. G. Hornby, "Multicenter randomized clinical trial evaluating the effectiveness of the lokomat in subacute stroke," *Neurorehabilitation and Neural Repair*, vol. 23, no. 1, pp. 5–13, 2009.

[13] J. Meuleman, *Design of a robot-assisted gait trainer: LOPES II*. PhD thesis, 2015.

[14] J. Patton, D. A. Brown, M. Peshkin, J. J. Santos-Munn, A. Makhlin, E. Lewis, E. J. Colgate, and D. Schwandt, "KineAssist: design and development of a robotic overground gait and balance therapy device," *Topics in Stroke Rehabilitation*, vol. 15, pp. 131–139, March-April 2008.

[15] N. Hogan, "Impedance control: An approach to manipulation," in *American Control Conference, 1984*, pp. 304–313, IEEE, 1984.

[16] E. Colgate and N. Hogan, "An analysis of contact instability in terms of passive physical equivalents," in *Robotics and Automation, 1989. Proceedings., 1989 IEEE International Conference on*, pp. 404–409, IEEE, 1989.

[17] J. Kang, V. Vashista, and S. K. Agrawal, "On the adaptation of pelvic motion by applying 3-dimensional guidance forces using tpad," *IEEE Transactions on Neural Systems and Rehabilitation Engineering*, vol. 25, no. 9, pp. 1558–1567, 2017.

[18] D. Aoyagi, W. E. Ichinose, S. J. Harkema, D. J. Reinkensmeyer, and J. E. Bobrow, "A robot and control algorithm that can synchronously assist in naturalistic motion during body-weight-supported gait training following neurologic injury," *IEEE Transactions on Neural Systems and Rehabilitation Engineering*, vol. 15, no. 3, pp. 387–400, 2007.

[19] A. Olenek, M. Zadravec, and Z. Matjai, "A novel robot for imposing perturbations during overground walking: mechanism, control and normative stepping responses.," *Journal of neuroengineering and rehabilitation*, vol. 13, p. 55, June 2016.

[20] J. A. M. Haarman, M. Vlutters, R. A. C. M. Olde Keizer, E. H. F. van Asseldonk, J. H. Buurke, J. Reenalda, J. S. Rietman, and H. van der Kooij, "Paretic versus non-paretic stepping responses following pelvis perturbations in walking chronic-stage stroke survivors.," *Journal of neuroengineering and rehabilitation*, vol. 14, p. 106, Oct. 2017.

[21] G. Brown, M. M. Wu, F. C. Huang, and K. E. Gordon, "Movement augmentation to evaluate human control of locomotor stability," in *Proc. 39th Annual Int. Conf. of the IEEE Engineering in Medicine and Biology Society (EMBC)*, pp. 66–69, July 2017.

[22] B. Vanderborght, A. Albu-Schäffer, A. Bicchi, E. Burdet, D. G. Caldwell, R. Carloni, M. Catalano, O. Eiberger, W. Friedl, G. Ganesh, *et al.*, "Variable impedance actuators: A review," *Robotics and autonomous systems*, vol. 61, no. 12, pp. 1601–1614, 2013.

[23] J. Pratt, B. Krupp, and C. Morse, "Series elastic actuators for high fidelity force control," *Industrial Robot: An International Journal*, vol. 29, no. 3, pp. 234–241, 2002.

[24] H. Vallery, J. Veneman, E. Van Asseldonk, R. Ekkelenkamp, M. Buss, and H. Van Der Kooij, "Compliant actuation of rehabilitation robots," *Robotics & Automation Magazine, IEEE*, vol. 15, no. 3, pp. 60–69, 2008.

[25] K. Kong, J. Bae, and M. Tomizuka, "A compact rotary series elastic actuator for human assistive systems," *Mechatronics, IEEE/ASME Transactions on*, vol. 17, no. 2, pp. 288–297, 2012.

[26] J. F. Veneman, R. Ekkelenkamp, R. Kruidhof, F. C. van der Helm, and H. van der Kooij, "A series elastic-and bowden-cable-based actuation system for use as torque actuator in exoskeleton-type robots," *The international journal of robotics research*, vol. 25, no. 3, pp. 261–281, 2006.

[27] H. Yu, S. Huang, G. Chen, Y. Pan, and Z. Guo, "Human–robot interaction control of rehabilitation robots with series elastic actuators," *IEEE Transactions on Robotics*, vol. 31, no. 5, pp. 1089–1100, 2015.

[28] N. Dominici, U. Keller, H. Vallery, L. Friedli, R. van den Brand, M. L. Starkey, P. Musienko, R. Riener, and G. Courtine, "Versatile robotic interface to evaluate, enable and train locomotion and balance after neuromotor disorders," *Nature medicine*, vol. 18, no. 7, pp. 1142–1147, 2012.

[29] H. Vallery, P. Lutz, J. Von Zitzewitz, G. Rauter, M. Fritschi, C. Everarts, R. Ronsse, A. Curt, and M. Bolliger, "Multidirectional transparent support for overground gait training," in *Rehabilitation Robotics (ICORR), 2013 IEEE International Conference on*, pp. 1–7, IEEE, 2013.

[30] H. Vallery, A. Duschau-Wicke, and R. Riener, "Hiding robot inertia using resonance," in *Engineering in Medicine and Biology Society (EMBC), 2010 Annual International Conference of the IEEE*, pp. 1271–1274, IEEE, 2010.

[31] W. Zijlstra and A. L. Hof, "Displacement of the pelvis during human walking: experimental data and model predictions," *Gait & posture*, vol. 6, no. 3, pp. 249–262, 1997.

[32] J. H. Meuleman, R. Kruithof, E. H. van Asseldonk, and H. van der Kooi, "Pilot study on following and resisting forces on the pelvis," in *Converging Clinical and Engineering Research on Neurorehabilitation*, pp. 147–152, Springer, 2013.

[33] H. Vallery, A. Bgel, C. O'Brien, and R. Riener, "Cooperative Control Design for Robot-Assisted Balance during Gait," *at-Automatisierungstechnik*, vol. 60, no. 11, pp. 715–720, 2012.

[34] S. Huang and J. M. Schimmels, "The bounds and realization of spatial stiffnesses achieved with simple springs connected in parallel," *Robotics and Automation, IEEE Transactions on*, vol. 14, no. 3, pp. 466–475, 1998.

[35] S. M. Bruijn, O. G. Meijer, P. J. Beek, and J. H. van Dieën, "The effects of arm swing on human gait stability," *The Journal of experimental biology*, vol. 213, no. 23, pp. 3945–3952, 2010.

[36] G. Wyeth, "Control issues for velocity sourced series elastic actuators," in *Proceedings of the Australasian Conference on Robotics and Automation 2006*, Australian Robotics and Automation Association Inc, 2006.

[37] J. H. Meuleman, E. H. van Asseldonk, and H. van der Kooij, "The effect of directional inertias added to pelvis and ankle on gait," *Journal of neuroengineering and rehabilitation*, vol. 10, no. 1, p. 40, 2013.

[38] C. K. Balasubramanian, R. R. Neptune, and S. A. Kautz, "Variability in spatiotemporal step characteristics and its relationship to walking performance post-stroke," *Gait & posture*, vol. 29, no. 3, pp. 408–414, 2009.

[39] S. J. Olney and C. Richards, "Hemiparetic gait following stroke. part i: Characteristics," *Gait & posture*, vol. 4, no. 2, pp. 136–148, 1996.

[40] B. Raja, R. R. Neptune, and S. A. Kautz, "Coordination of the non-paretic leg during hemiparetic gait: expected and novel compensatory patterns," *Clinical Biomechanics*, vol. 27, no. 10, pp. 1023–1030, 2012.

[41] H. P. von Schroeder, R. D. Coutts, P. D. Lyden, V. L. Nickel, *et al.*, "Gait parameters following stroke: a practical assessment," *Journal of rehabilitation research and development*, vol. 32, no. 1, p. 25, 1995.

[42] N. Neckel, D. Nichols, and J. Hidler, "Joint Moments Exhibited by Chronic Stroke Subjects While Walking with a Prescribed Physiological Gait Pattern," in *Proceedings of the IEEE International Conference on Rehabilitation Robotics (ICORR)*, pp. 771–775, 2007.

[43] M. Pietrusinski, I. Cajigas, G. Severini, P. Bonato, and C. Mavroidis, "Robotic gait rehabilitation trainer," vol. 19, pp. 490–499, Apr. 2014.

[44] P. Beckerle, T. Verstraten, G. Mathijssen, R. Furnémont, B. Vanderborght, and D. Lefeber, "Series and parallel elastic actuation: Influence of operating positions on design and control," *IEEE/ASME Transactions on Mechatronics*, vol. 22, no. 1, pp. 521–529, 2017.

[45] J. van der Weijde, E. Vlasblom, P. Dobbe, H. Vallery, , and M. Fritschi, "Force sensing for compliant actuators using coil spring inductance," in *proceedings of the IEEE/RSJ International Conference on Intelligent Robots and Systems (IROS)*, (Hamburg), 2015.

[46] A. L. Hof, "The 'extrapolated center of mass' concept suggests a simple control of balance in walking," *Human Movement Science*, vol. 27, pp. 112–125, 2008.

[47] J. Pratt, J. Carff, and S. Drakunov, "Capture point: A step toward humanoid push recovery," in *Proceedings of the IEEE-RAS International Conference on Humanoid Robots (HUMANOIDS)*, 2006.

[48] A. Pennycott, D. Wyss, H. Vallery, and R. Riener, "Effects of added inertia and body weight support on lateral balance control during walking," in *Rehabilitation Robotics (ICORR), 2011 IEEE International Conference on*, pp. 1–5, IEEE, 2011.

[49] D. Wyss, V. Bartenbach, A. Pennycott, R. Riener, and H. Vallery, "A body weight support system extension to control lateral forces: Realization and validation," in *Robotics and Automation (ICRA), 2014 IEEE International Conference on*, pp. 328–332, IEEE, 2014.

Dario Wyss received the M.Eng. in mechanical engineering from ETH Zurich in 2011. In 2012 he joined the Sensory-Motor Systems Lab. His research interests include compliant actuation principles applied to rehabilitation and assistive robotics.

Andrew Pennycott received the M.Eng. and the Ph.D. degrees in mechanical engineering from the University of Glasgow in 2004 and 2008, respectively. His research is focused on control engineering for automotive and rehabilitation applications.

Volker Bartenbach received a diploma in engineering in 2010 from Karlsruhe Institute of Technology (KIT), Germany, after writing his thesis on adaptive knee prostheses. In 2012 he joined the Sensory-Motor Systems Lab at ETH Zurich for his PhD project on lower-limb exoskeletons. In 2017 he was awarded an ETH Pioneer Fellowship and joined the Rehabilitation Engineering Lab to start working on industrial exoskeletons.

Robert Riener is full professor for Sensory-Motor Systems at the Department of Health Sciences and Technology, ETH Zurich, and full professor of medicine at the University Hospital Balgrist, University of Zurich. He obtained a MSc in mechanical engineering in 1993 and a PhD in biomedical engineering 1997, both from TU München, Germany. Since 2003 he is professor in Zurich. Riener has published more than 400 peer-reviewed articles, 20 book chapters and filed 23 patents. He is the initiator and organizer of the Cybathlon.

Heike Vallery is a full professor at the faculty of Mechanical, Maritime and Materials Engineering, TU Delft. She received her Dipl.-Ing. degree (with honors) in mechanical engineering from RWTH Aachen in 2004, and a Ph.D. from TU München in 2009. Her research interests include bipedal locomotion, compliant actuation, and rehabilitation. She has received numerous fellowships and awards, such as the 1st prize of the euRobotics Technology Transfer Award 2014, and a Vidi fellowship in 2016 from the Netherlands Organisation for Scientific Research.